

Organic-Inorganic Films with Anticorrosive and Bactericidal Properties for Titanium Implants

C.K.C. Kayser^a, L.T. Mueller^a, L.G. Soares^{a*} , D.R. Volz^b , A.L. Ziulkoski^b , E.L. Schneider^c ,
C.T. Oliveira^a , F.D.P. Morisso^a, S.R. Kuns^a , C.L.P. Carone^a

^aUniversidade Feevale, Instituto de Ciências Criativas e Tecnológicas (ICCT), Laboratório de Estudos Avançados em Materiais, Bairro Vila Nova, 93352-000, Novo Hamburgo, RS, Brasil.

^bUniversidade Feevale, Instituto de Ciências da Saúde (ICS), Laboratório de Citotoxicidade, Bairro Vila Nova, 93352-000, Novo Hamburgo, RS, Brasil.

^cUniversidade Federal do Rio Grande do Sul (UFRGS), Departamento de Metalurgia, Laboratório de Metalurgia Física (LAMEF), Programa de Pós-Graduação em Engenharia de Minas, Metalúrgica e de Materiais, Bairro Agronomia, 91500-970, Porto Alegre, RS, Brasil.

Received: April 26, 2023; Revised: October 20, 2023; Accepted: October 31, 2023

This study seeks to synthesize, by the sol-gel method, an organic-inorganic hybrid coating of polyurethane, siloxane and silver nanoparticles to cover titanium prostheses, aiming to act as an anticorrosive protection barrier, inhibiting the release of metallic ions in the human body. In this context, a hybrid based on the TEOS (tetraethyl orthosilicate) alkoxide precursor was used to carry out the acid hydrolysis/condensation process. Then, silver nanoparticles were added, and the mixture was done with the incorporation of polycaprolactone diol, followed by the addition of hexamethylene diisocyanate, to form polyurethane. The hybrid coatings were applied on titanium plates, and morphological, physical-chemical and electrochemical characterizations were carried out, as well as the evaluation of bactericidal and antifungal activity, in order to evaluate the performance of the coatings and the influence of different concentrations of silver nanoparticles (10 mL, 20 mL and 40 mL). The results showed that although Híbrido 10 (lowest concentration of silver nanoparticles, 10 mL) presented the best morphological characteristic without cracks and with satisfactory roughness to obtain the best bacterial behavior, the Híbrido 20 sample presented the best electrochemical performance.

Keywords: Polyurethane, Silver nanoparticle, Coating, Sol-gel, Titanium prostheses, Corrosion.

1. Introduction

Polyurethanes are polymers that have very diverse applicability. They can be foams, elastomers, paints, coatings, varnishes, adhesives and sealants. These polymers have enough flexibility to generate materials with different physical and chemical properties, consequently making them synthetic polymers with high performance and versatility. Studies demonstrate that polyurethane can be used to obtain hybrid coatings, and that fillers have been used to improve the different properties of polyurethane-based coatings^{1,2}.

Studies reveal that organic-inorganic hybrid coatings prepared via the sol-gel process are possible substitutes for some current protective coatings, since they act as corrosion inhibitors by forming a chemically inert barrier against the diffusion of species that initiate corrosive processes³. Silanes are generally used as hybrid coating precursors, because when applied to metallic surfaces, they form a reticulated film that inhibits or delays the corrosion process^{4,5}.

In addition, the strict control of the parameters of the sol-gel formation reactions allows the design of new materials with interesting properties for many applications, with emphasis on the retardation of the corrosive process⁶.

Among the many polymeric materials for use in the preparation of resins via the sol-gel process, polyurethanes can be highlighted, which are widely used in coatings, dressings, textiles, leather, adhesives, liquid crystals and nanobiomaterials. Cross-linked siloxane-polyurethane for example, are widely used in marine coatings as a scale inhibitor⁷.

Another important factor regarding metal surfaces is that they are an appropriate environment for bacterial adhesion and proliferation, enabling the formation of biofilm. Infections caused by biofilm-forming microorganisms are a major problem in the medical field. The main sources of transmission of bacterial pathogens in hospitals are related to the contact with contaminated surfaces and medical equipment. Consequently, with the contamination of hands, gloves and prostheses, these pathogenic microorganisms are transmitted to hospitalized patients⁸⁻¹⁰. Antibacterial agents have been used to control the number of infections in the hospital environment, since they are able to slow down the growth of certain bacteria or even cause their death. Surface modification has been widely used to provide antibacterial properties to material surfaces. Among the surfaces that have a bactericidal effect are those with silver in their composition¹¹⁻¹³.

Since ancient times, silver has been known for its antibacterial properties. Its antibacterial property results from the constant and prolonged release of silver ions.

*e-mail: lugoess.soares@gmail.com

When they are at a nanometric scale, their properties are enhanced, as their reduced size and greater surface/volume ratio favor penetration through the membrane of bacterial cells, thus improving their performance as a bactericidal agent^{14,15}. Polyurethanes are also a great option for use in antimicrobial coatings, due to their good mechanical properties and biocompatibility^{16,17}.

2. Experimental

2.1. Materials

The reagents were used as received and are commercially available, they are: polycaprolactonediol (Sigma Aldrich), N,N-dimethylformamide (DMF, Synth), 1,6-hexamethylene diisocyanate (Sigma Aldrich), dibutyl tin dilaurate (Sigma Aldrich), tetraethoxysilane (Sigma Aldrich), ethyl alcohol (Modern Chemistry), deionized water, hydrochloric acid (Dinâmica) and sodium borohydride (Home of Chemistry).

Table 1 presents the technical information of the reagents used in this work. The silver nitrate used was a 0.05 M solution available at Feevale's Laboratory for Advanced Studies in Materials.

2.2. Synthesis of silver nanoparticles

To synthesize the AgNPs, a chemical reduction of AgNO_3 was performed, using sodium borohydride as reducing/stabilizing agent¹⁸. A 4.0×10^{-3} M solution of sodium borohydride and a 2.0×10^{-3} M solution of silver nitrate were prepared. Silver nanoparticles were synthesized at three different concentrations. Different volumes of AgNO_3 solution were added drop by drop at a rate of 1 drop per second: 10, 20 and 40 mL. This addition was carried out in 50 mL of sodium borohydride, with constant stirring. The three prepared solutions were named, respectively, solution 1, 2 and 3. Thus, assuming the complete reduction of the Ag^+ ion to Ag^0 particles (AgNPs), the final concentrations of solutions 1, 2 and 3 were 3.0×10^{-4} M, 5.71×10^{-4} M and 8.88×10^{-4} M, respectively. These solutions showed a yellowish color, and their electronic spectra were immediately obtained to confirm the formation of nanoparticles. Remembering that electronic spectrum is a set of transitions, absorptions or emissions, between electronic states.

2.3. Synthesis of the siloxane-polyurethane-silver hybrid

The synthesis of the siloxane-polyurethane-silver hybrid was divided into three steps. In the first stage, a silica network was formed via the hydrolysis and condensation reactions

of TEOS (Tetraethyl orthosilicate) by acid catalysis. In this step TEOS (2.5 mL, 11.3 mMol) was mixed with ethanol (6 mL, 103 mMol) at room temperature using magnetic stirring. Afterward, water (1.5 mL, 83 mMol) was added in small amounts, and the pH of the mixture was adjusted with hydrochloric acid to pH = 2. The mixture was stirred constantly for 10 minutes, obtaining a transparent solution¹⁹.

In the second stage, the synthesis of the hybrid was performed²⁰. To synthesize the organic-inorganic hybrid using the sol-gel process, polycaprolactone diol was first dissolved using DMF (N,N-Dimethylformamide). The pre-hydrolyzed TEOS mixture was added, then the system was kept at 70°C using constant agitation for 1 hour.

Then the third stage began, when the polyurethane formation reaction occurred by the in-situ polymerization method. In this step, the slow addition of HDI (Hexamethylene diisocyanate) was performed in the presence of DBTL (Dibutyltin dilaurate). The reaction occurred for 1 hour and 30 minutes under inert nitrogen atmosphere using reflux. The NCO:OH ratio used in this synthesis was 1.7:1, and the molar amount of TEOS was added to the excess of NCO, i.e. 0.7 mol of TEOS. Using this methodology, a hybrid coating was obtained, which was named "Pure Hybrid". Three more coatings containing silver nanoparticles were synthesized by the same methodology. In this sense, 3 mL of solution 1 were added to 10 mL of the translucent siloxane solution prepared in the first stage of synthesis resulting in a siloxane/Ag solution containing 6.92×10^{-5} M of AgNPs, which was added to the polycaprolactone diol/DMF solution during the second stage of synthesis. Then, the synthetic pathway was followed as for Pure Hybrid. The same strategy was applied with solutions 2 and 3, resulting in 1.32×10^{-4} M and 2.03×10^{-4} M of AgNPs solutions, respectively. The PU/siloxane hybrids containing AgNPs were named "Hybrid 10", "Hybrid 20" and "Hybrid 40".

2.4. Deposition on the substrate

This study used CP titanium samples (plates), graded 2 and measuring approximately 2x3 cm. The plates were pickled in a 60:40% HNO_3 :HF solution for 10 seconds, then rinsed with deionized water. A milled sheet of c.p. titanium grade 2 was acquired from the company Titânio Brasil Ltda with a thickness of 1 mm and roughness of 31.6 ± 0.41 nm. The samples were cut from the plate, in a rectangular shape, with a width of 4.5 cm and a length of 5.1 cm (anodized area of 45.9 cm²). After pickling, the hybrids was deposited on the titanium plates using dip coating at room temperature.

Table 1. Technical information of the reagents used.

Reagents	Acronym	P. M. (g/mol)	Purity (%)	Supplier
Polycaprolactonediol	PCL	~2000	-	Sigma Aldrich
N,N-Dimethylformamide	DMF	73.09	99.8	Synth
1,6 – Hexamethylene diisocyanate	HDI	168.19	≥98.0	Sigma Aldrich
Dibutyl tin dilaurate	DBTL	631.56	95.0	Sigma Aldrich
Tetraethoxysilane	TEOS	208.33	98.0	Sigma Aldrich
Ethyl alcohol	$\text{CH}_3\text{CH}_2\text{OH}$	46.07	99.5	Modern Chemistry
Hydrochloric acid	HCl	36.46	-	Dynamics
Sodium borohydride	NaBH_4	37.83	97.0	Home of Chemistry

Each titanium plate was immersed in a hybrid at a speed of 14 cm/min for 1 minute. They were dried for 30 minutes at 60°C. After drying, each titanium plate was immersed in a hybrid again, under the same conditions used previously. Finally, the materials were cured for 30 minutes at 150 °C.

2.5. Evaluation of bactericidal and antifungal activity

For the evaluation of biofilm formation on metallic mini plates, bacterial strains (*Escherichia coli* ATCC 25922, *Pseudomonas aeruginosa* ATCC 27853, *Staphylococcus aureus* ATCC 12598) and a fungal strain (*Candida albicans* ATCC 10231) were cultured in blood agar. In the following 24 hours, the strains were used to prepare the inoculum for the formation of the biofilm; these inocula were prepared with Mueller Hinton agar, with a McFarland standard close to 0.5, which is equivalent to 1.5×10^8 CFU/mL (colony forming units). Metal plates were fixed on sterile cell culture plates covered with 400 μ L Mueller Hinton agar, and approximately 30 min later 400 μ L of inoculum were added, covering the upper surface of the metal plates. The plates were then incubated in an oven (36°C) for 24h. Afterwards, the metal plates were flexible using sterile tweezers to new cell culture plates, where they were uncovered by 500 μ L of Mueller Hinton Broth and remained in an oven for 72 hours. When the 48 hours of incubation were completed, the metal plates were stained with crystal violet. To this end, 400 μ L of 4% formaldehyde were added for fixation during 15 min. Then, using a micropipette, the liquid part was removed, and the dye was added using various volumes so that the surface of the miniplates covered around 400-600 μ L, for 30 min. After this period, excess crystal was removed using absorbent paper, and the miniplates were placed externally in other cell culture wells. For solubilization, 300 μ L of absolute ethyl alcohol were added and analyzed at a length of 580 nm by a spectrophotometer. Considering that the fixed violet dye sets on the cell membranes, the intensity of their color is directly proportional to the number of microorganisms present on the metal plates.

2.6. Characterizations

Infrared vibrational spectroscopy was performed at room temperature, using a Perkin Elmer Spectrum spectrophotometer, version 10.4.2. Each spectrum was obtained by the accumulation of 4 scans, with beam incidence in the infrared region in the range of 4000 to 450 cm^{-1} . Samples were analyzed for morphology in a top view perspective, and EDS (energy dispersive spectroscopy) and chemical mapping was performed. The equipment used for these analyzes was a SEM, model JEOL JSM-6510LV. To obtain the images by atomic force microscopy (AFM), a Park Systems XE7 microscope was used in contact mode, with a non-contact cantilever tip (model PPP-NCHR) 10M and a scanning area of 10 x 10 μm . The evolution of surface roughness was evaluated by mean roughness measurements (R_a). Before the electrochemical potentiodynamic polarization assay, the OCP (open circuit potential) was monitored for 5 minutes. The electrochemical potentiodynamic polarization assay was performed with a 1 mV/s sweep, starting at -200 mV and reaching +400 mV, with respect to OCP in a simulated body fluid (SBF) electrolyte (pH 7.4) and at room temperature.

Samples were tested in triplicate and the equipment used was a Potentiostat PGSTAT302, AUTOLAB.

3. Results and Discussion

3.1. Structural analysis

The hybrids, pure and with the addition of different concentrations of silver nanoparticles, were analyzed by infrared spectroscopy. Figure 1 shows the spectra of the superimposed films. The bands were assigned in relation to the values of the characteristic frequencies existing in the literature regarding the groups.

Evaluating the spectra presented in Figure 1, it can be seen that polyurethane was formed without excess diisocyanate in the medium, since no absorption happened in the region from 2280 cm^{-1} to 2000 cm^{-1} , showing that there is no cumulative double bond typical of the cyanide group (NCO). Furthermore, it can be confirmed that PCL was converted into polyurethane due to the presence of the band in the 1700 cm^{-1} region, which is characteristic of the carbonyl group (C=O). The absorption occurring between 3200 and 3700 cm^{-1} is characteristic of the axial deformation of the OH, which can arise due to the presence of non-condensed silanol groups (Si-OH) during the curing of the films. The peaks in the 2900 cm^{-1} region are representative of the axial deformation of the C-H bond of the CH_2 and CH_3 groups. Between 1000 and 1200 cm^{-1} , intense bands attributed to the Si-O-Si bond can be noticed, which are the main bonds of the film structure based on the alkoxy-silanes responsible for barrier protection^{21,22}. The bands in the region from 900 to 960 cm^{-1} indicate the presence of Si-OCH₂CH₃ resulting from the incomplete hydrolysis of the TEOS silane. Assessing the spectra, it can be stated that a hybrid with TEOS was formed. The bonds of the siloxane with the polymer were confirmed by infrared analysis. TGA studies have shown that increasing the siloxane crosslinking increases the thermal stability of the resulting films, which is evidenced by the activation energy values. Contact angle studies showed that it had an increase in its hydrophobicity²³.

In Figure 2, this can be verified due to the reaction that takes place during the curing process of the hybrid coatings.

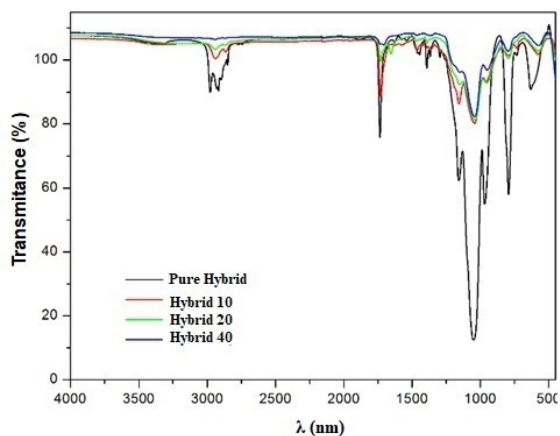


Figure 1. Infrared spectra of hybrids.

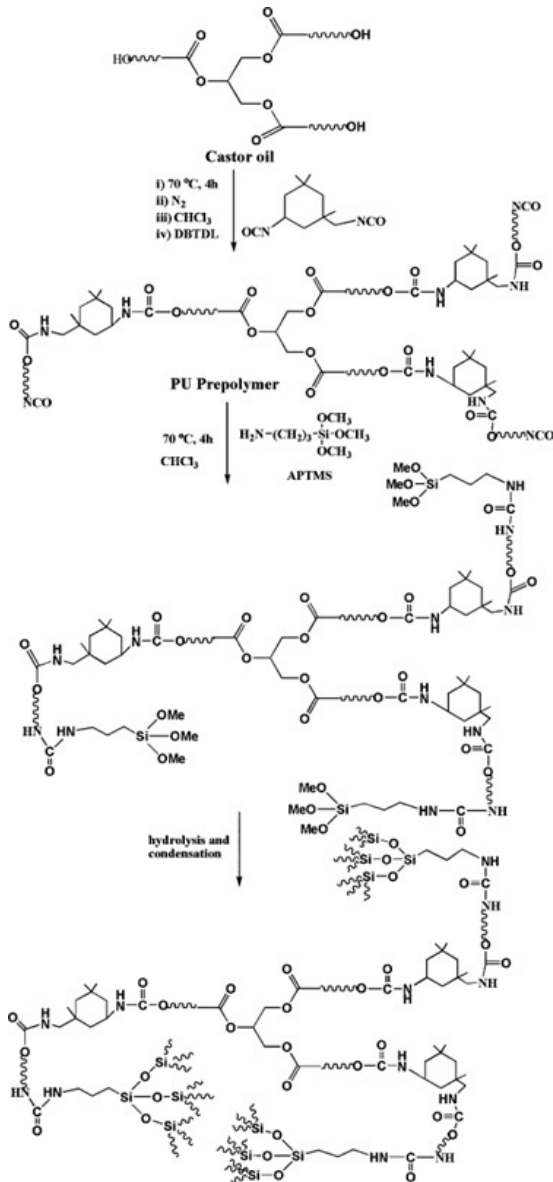


Figure 2. Cross-Linked Structures⁷.

All synthesized samples showed a very small band referring to the axial O-H deformation of the Si-OH group, which attests to the condensation of the groups. Thus, theoretically, the synthesized hybrids have good stability and barrier function. A researcher has developed hybrid siloxane-poly (methyl methacrylate) (PMMA) coatings via the copolymerization between the methacrylate groups of Methacryloxy Propyl Trimethoxy Silane and methyl methacrylate, followed by the acid hydrolysis/polycondensation of the tetraethoxy-silane systems and the addition of different concentrations of molybdenum. Using Fourier-transform infrared spectroscopy (FTIR), the author verified that the inclusion of molybdenum in the hybrid made the band around 1150 cm^{-1} more intense, suggesting that the addition of molybdenum salt improves the barrier protection of the film²⁴.

In this study, the addition of silver nanoparticles decreased the intensity of the band between 1000 and 1200 cm^{-1} . In Figure 1, it can be observed that the Pure Hybrid has a much higher intensity in the 1000 - 1200 cm^{-1} band than the hybrids containing silver nanoparticles. Some authors report that higher concentrations of siloxane bonds lead to improved corrosion protection²⁵⁻²⁷.

In addition to polyurethane and siloxane, the AgNPs are added to three different concentrations. The FTIR results show that the presence of silver nanoparticles did not alter the structural composition of the hybrid, but it considerably reduced the peak intensity between 1000 and 1200 cm^{-1} attributed to the Si-O-Si bond, as previously mentioned. Researchers studied a silver hydroxyapatite coating for application to stainless steel to improve corrosion resistance and antibacterial properties. The functional groups of the coatings without and with added silver were studied using FTIR, and the results showed that the presence of silver nanoparticles did not alter the structural composition of hydroxyapatite^{28,29}. Palza³⁰ studied the mechanism of antibacterial activity of metallic nanoparticles incorporated into dense polymeric matrices such as thermoplastics and concluded that the release of ions is the main mechanism behind the antimicrobial activity. A study carried out using X-ray photoelectron spectroscopy (XPS) showed that nanoparticles are not present on the surface of the material, but rather in its bulk (i.e., being connected to the property of material volume). Afterward, the material was placed in contact with water, and metallic ions were verified on the surface, demonstrating that only the ions were diffused. Even highly nonpolar matrices, such as polyethylene, allow the diffusion of water molecules. Therefore, the only adequate mechanism for the release of metallic ions is the leaching present in the polymer bulk, due to the diffusion of water molecules from the bacterial environment to the surface of the nanoparticles.

3.2. Scanning electron microscopy and chemical mapping analysis (top)

Figure 3 presents the micrographs obtained by SEM of the CP titanium (CP Ti) and hybrid film samples, at $500\times$, $1000\times$ and $5000\times$ magnifications, respectively. Figure 3a shows the surface of the CP titanium, where some irregularities can be seen, which result from the manufacturing process of the titanium plate. In addition, these imperfections may also be associated with the surface oxide of the metal, which is a natural and unstable oxide that forms on pure titanium when exposed to oxygen at room temperature. This oxide layer formed on the surface of pure titanium grows spontaneously, consisting mainly of TiO_2 and Ti_3O_5 . This layer is a few nanometers thick and follows the topography of the metal, which has an irregular surface³¹. However, when CP titanium is applied to joints and/or prostheses, this oxide layer is not effective enough to protect CP Ti in some aggressive environments, due to its thin layer with low wear resistance³². The speed at which titanium oxidation and, consequently, the formation of the oxide layer occur depends on the conditions of the environment, and can take place in anaerobiosis, where the oxidizing agent is water, and in aerobiosis, where the oxidizing agent is oxygen.

At the same time, the surface of titanium implants and their alloys can form favorable environments for bacterial adhesion and proliferation, facilitating the development of a drug-resistant biofilm^{33,34}. Figure 3b shows the pure hybrid coating on a titanium plate. This coating had good homogeneity and covered the imperfections of the titanium. When comparing all tested coatings, it can be observed that the pure hybrid had the most regular surface with no microcracks in the film, covering only the imperfections of the titanium surface, suggesting that the coating promoted good adhesion³⁵. When the coating has good coverage and adhesion to the substrate, the surface morphology changes after the film is applied, as the film covers the entire surface evenly, and grooves or markings on the surface of the substrate are smoothed out, as evidenced by the pure hybrid coating³⁶. Figures 3c-e show the micrographs obtained from the Hybrid 10, Hybrid 20 and Hybrid 40 coatings, respectively. The addition of a small amount of silver (Hybrid 10) results in the formation of a homogeneous film, without recesses and with slight discontinuities. However, it is observed that the Hybrid 20 and Hybrid 40 samples have cracks on the surface

of the layer. That is, at higher silver concentrations, a lack of interactions between the first and second coating layers was observed. This may be associated with the long interval between the two immersions (30 minutes at 60°C), this sample preparation can be adjusted to allow for a higher concentration of silver nanoparticles without weakening the film. However, due to the fragility of the thicker layers, microcracks can be observed in its morphology and, consequently, this film will have a decrease in corrosion resistance. Furthermore, the formation of an irregular first layer prevents the formation of a second layer^{20,37}: as shown in Figure 3d, the second layer of Hybrid 20 failed to adhere to the first layer. Kayani et al.³⁸ studied the effect of different silver concentrations on ZnO (zinc oxide) thin films prepared by the sol-gel process. According to the morphological analysis of the films, the authors observed that the increase in the percentage of silver generates a film with a surface with greater irregularities and with silver agglomerates, when compared to a film with a lower concentration of silver. This is consistent with the surface of the Hybrid 40 sample, where there is a higher concentration of silver and clusters can be observed³⁹.

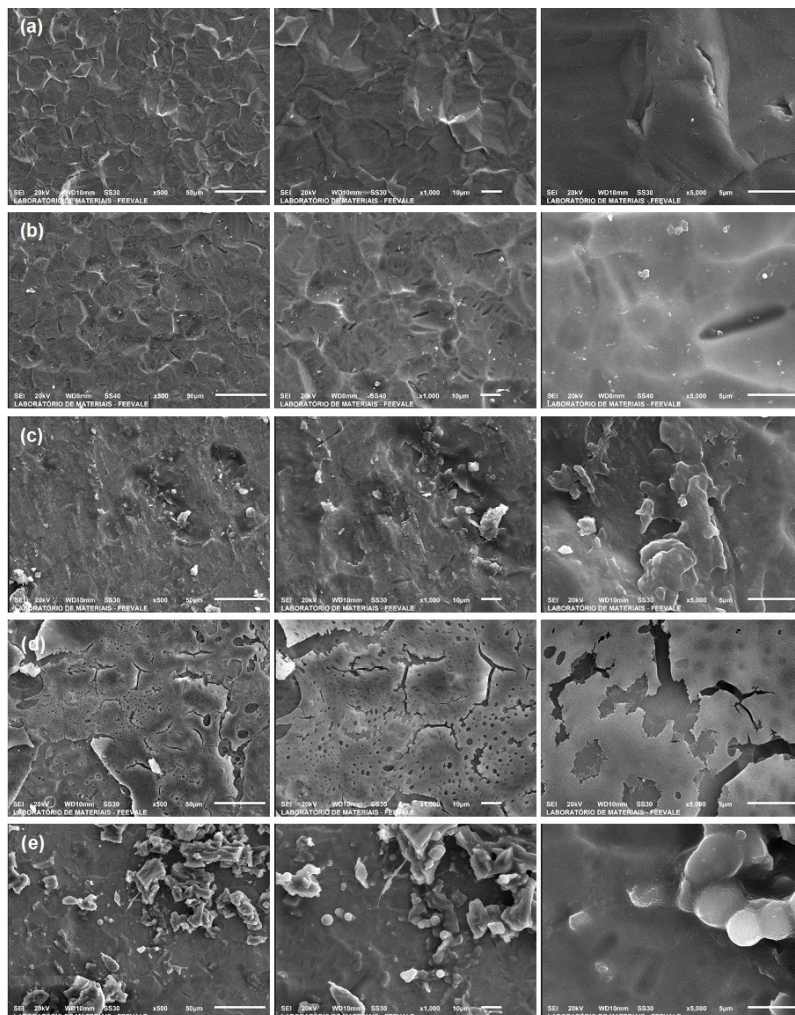


Figure 3. Micrographs obtained by SEM in top view of the titanium samples under the following conditions: a) CP titanium; b) Pure hybrid; c) Hybrid 10; d) Hybrid 20; e) Hybrid 40.

Figure 4 shows chemical mapping of the hybrid. The chemical mapping analysis of the surface of the pure hybrid film indicates the presence of oxygen, carbon, silicon and titanium. In the hybrid films with inserted silver nanoparticles – Hybrid 10, Hybrid 20 and Hybrid 40 –, the presence of oxygen, carbon, silicon and titanium in addition to silver was also detected, as shown in Figure 4.

Among these materials, the one with the highest amount of silicon was Hybrid 20, and it was the system with the highest number of cracks in its coating. This is due to the fact that the TEOS-based silane precursor tends to form a compact three-dimensional network, generating new networks to the detriment of polyurethane (PU). In this way, the PU is completely encapsulated by various forces (hydrogen, Van der Waals or covalent bonds), restricting the mobility of small branches of the film⁴⁰ that is necessary for the absorption of mechanical energy. This results in a brittle film, as is shown in Figure 4c. When evaluating the silver distribution of the samples, it can be noticed that Hybrid 10 has a homogeneous distribution over its entire surface, which indicates that the silver incorporation process was efficient despite having a lower amount of silicon Figure 4b, which may impair anti-corrosion performance. However, the higher the silver concentration, the worse its distribution in the film. According to researchers, the insertion of silver nanoparticles occurs preferentially in rough surfaces. In addition, the concentration of AgNO_3 used in the synthesis of nanoparticles has a direct influence on the size, distribution and amount of the silver nanoparticles that were incorporated into the coating. The use of a smaller amount of AgNO_3 in the synthesis of AgNPs generates a surface with silver nanoparticles more uniformly

distributed on the surface compared to samples in which silver nanoparticles with a higher amount of AgNO_3 were used. Furthermore, the greater the amount of silver nitrate, the greater the probability of forming a coating with an agglomerated surface⁴¹.

3.3. Roughness analysis by atomic force microscopy

Figure 5 presents the three-dimensional images obtained by atomic force microscopy (AFM) for the pure hybrid, Hybrid 10, Hybrid 20 and Hybrid 40, respectively, and Table 2 show the mean roughness values of all tested coatings. The roughness of CP titanium surface can be attributed to the stability of the oxide there⁴². The application of the Pure Hybrid allowed the reduction of surface roughness, even if not significantly. Thus, the Pure Hybrid coating was able to smooth out the titanium substrate grooves. Some authors denote that surface roughness can interfere with the behavior of materials against corrosive processes. Generally, the higher the surface roughness parameter of a system, i.e. the rougher it is, the lower its resistance to corrosion, since surface roughness increases the contact area of the coating for the solutions that cause chemical attacks – in the case of biomaterials, body fluids –, thus accelerating the possible corrosion process and initially deteriorating the surface of the substrate⁴³. The electrochemical potential of a metallic implant varies according to the roughness of its surface, therefore, a rougher surface is less restrictive in relation to the release of electrons, resulting in a lower electrochemical potential⁴⁴. According to Figure 5 and Table 2, it can be observed that as the concentration of nanoparticles in the coating increases, the surface roughness also increases.

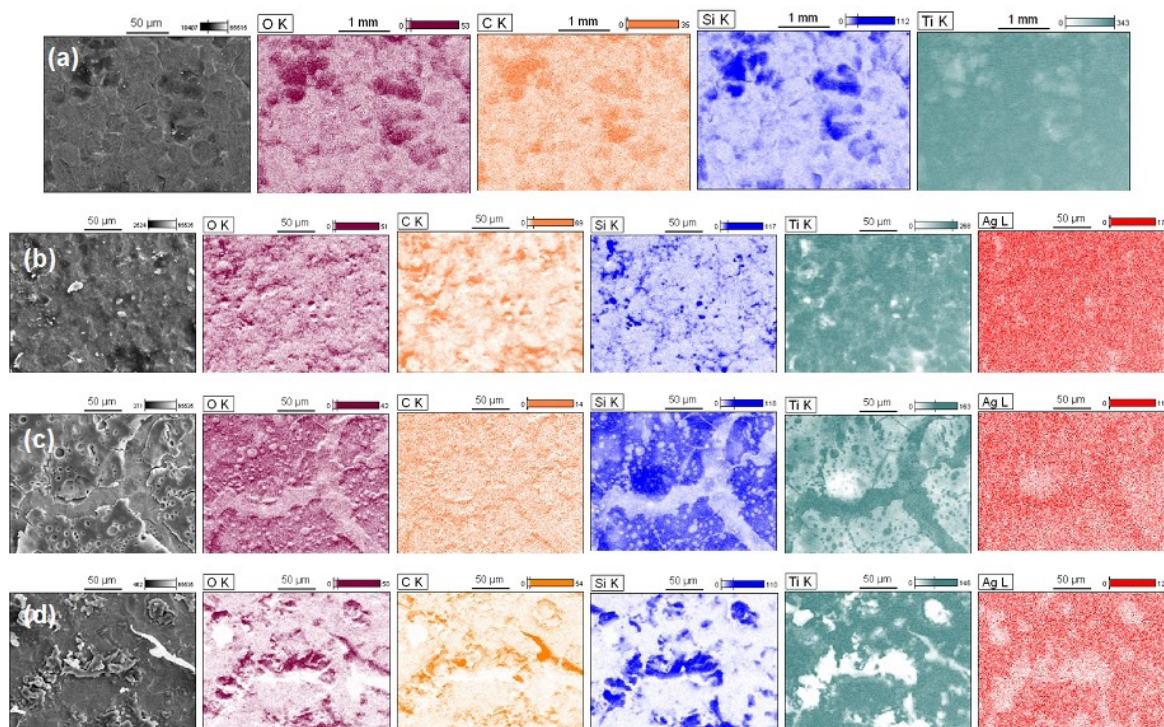


Figure 4. Chemical mapping of the hybrid coatings: a) Pure hybrid; b) Hybrid 10; c) Hybrid 20; d) Hybrid 40.

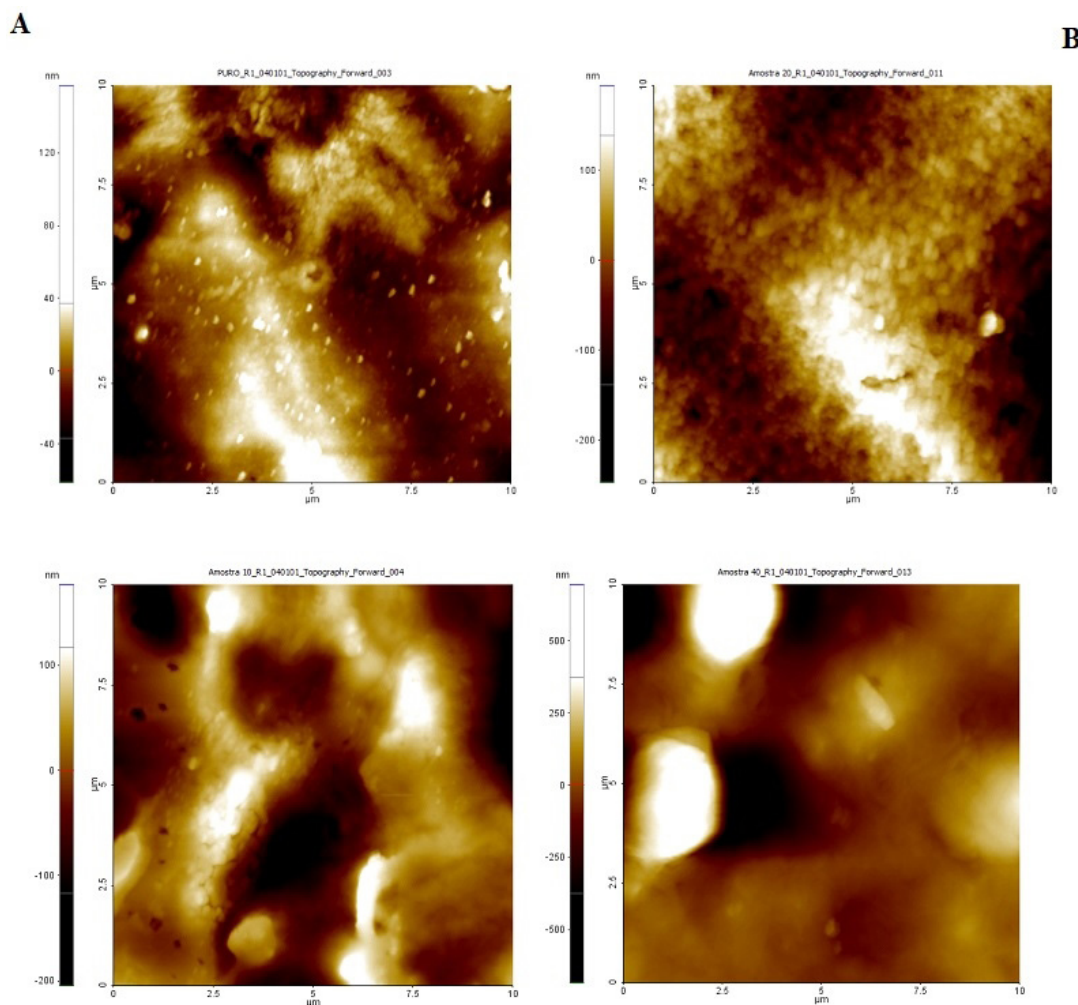


Figure 5. 2D AFM images of the surfaces of (a) Pure hybrid and (b) Hybrid 10 40.

Table 2. Mean roughness values obtained by AFM analysis.

Sample	Roughness (nm)
CP Titanium	31.6± 0.41
Pure Hybrid	30.0± 0.32
Hybrid 10	49.5± 0.37
Hybrid 20	57.2± 0.43
Hybrid 40	124.4± 0.81

Silver nanoparticles have always been a great candidate for inducing surface roughness, thus this behavior was expected. Longhi et al.⁴⁵, developed a superhydrophobic and antibacterial coating based on polydimethylsiloxane (PDMS) and silver phosphate. Anderson et al.⁴⁶ evaluated the influence of silver concentration, preparing coatings with 1% (1.58×10^{-4} M), 3% (4.74×10^{-4} M), 5% (7.90×10^{-4} M), 4 M) and 7% (1.11×10^{-3} M) silver content based on a 1 wt% polydimethylsiloxane (PDMS) solution. They found that the surfaces of the coatings became rougher as the silver nanoparticle content increased from 1 to 7% by weight. As the silver concentration increases, the nanoparticles

are more likely to adhere to each other, forming an interconnected, compact structure on the surface of the coating. The agglomeration of nanoparticles in the surface layer leads to the creation of cavities and grooves, reducing the solid/liquid contact area. Greater roughness does not increase protection against corrosive processes; however, when it comes to biomaterials, greater roughness allows for better biocompatibility. A smooth surface, without roughness, does not allow for good biocompatibility, since the *in vivo* integration of implants into bone tissue is related to an increase in the roughness of the implant surface, given that human osteoblasts adhere better to rough surfaces than to smooth ones⁴⁷. In view of this, from the point of view of biocompatibility, all coatings with silver nanoparticles have a rougher surface than CP titanium, i.e. they have a smaller contact area and, consequently, osseointegration is facilitated⁴⁸. In this context, a biomaterial with balanced aspects is sought, which has good resistance to corrosion due to the characteristics of its barrier film and has a surface roughness superior to that of CP titanium, therefore being able to improve the biocompatibility and osseointegration of implants, consequently reducing the rejection rate of these⁴⁹.

3.4. Potentiodynamic polarization

The results of the potentiodynamic polarization curves for c.p. titanium, as well as for hybrid coatings, are represented in Figure 6.

According to Figure 6, it is possible to identify that for potentials greater than the corrosion potential, an activation zone occurs with subsequent passivation for all samples. Furthermore, all hybrid coatings provided superior protective performance to c.p. titanium. For better interpretation of the potentiodynamic polarization results, the corrosion current density (i_{corr}) values were determined by the intersection of the anodic Tafel straight line with the cathodic Tafel straight line. Table 3 contains simulation data for the corrosion potential (E_{corr}), corrosion current (i_{corr}) and polarization resistance (R_p) of c.p. titanium and hybrid coatings.

The potentiodynamic polarization curve of the titanium c.p. sample shows the highest corrosion potential (-184.9 mV), corrosion current density of 6.99×10^{-6} A/cm² and polarization resistance of 5.85×10^{-2} Ω/cm², Table 3. Passivation of c.p. titanium occurs in a potential range from -0.1V to close to 0.1V at a passivation current density of approximately 10^{-4} A/cm².

When comparing the pure hybrid sample with cp titanium, Table 3, it is observed that the pure hybrid sample presents a variation of 3 orders of magnitude, with lower corrosion current density (6.32×10^{-9} A/cm²) and higher polarization resistance (4.06×10^5 Ω/cm²), demonstrating better anti-corrosion performance. This occurs because the pure Hybrid has a more homogeneous surface, as shown in the micrographs in Figure 3b. The corrosion protection mechanism for alkoxy-silane-based films is relatively simple, as it does not involve electrochemical protection. The protection of this type of film occurs through a physical barrier. The good barrier properties of the coatings are due to the development of a dense Si-O-Si network, which results in a compact and uniform film. This film slows down corrosion, preventing the passage of ions from the medium to the metal substrate, making it difficult for aggressive species to penetrate. In this way, the film acts as a hydrophobic barrier⁵⁰. The same electrochemical performance of the silane coating was verified on carbon steel. Rêgo et al.⁵¹ synthesized and evaluated, using electrochemical techniques, a hybrid coating of tetraethylorthosilicate/methacryloxypropyltrimethoxysilane/methyl methacrylate (TEOS/MPTS/MMA), obtained by the sol-gel process, with the purpose of delaying or reducing the corrosion process of a metallic surface. The hybrid coating was applied to carbon steel and presented a lower corrosion current density and more noble potential compared to uncoated carbon steel. The authors also attributed this behavior to the crosslinking of the silane film.

All coatings containing silver nanoparticles, Hybrid 10, Hybrid 20 and Hybrid 40, performed better than c.p. titanium, since they obtained lower corrosion current density. Comparing the Hybrid coatings without and with silver nanoparticles, Table 3, Hybrid 10 (1.19×10^{-8} A/cm²) and Hybrid 40 (1.18×10^{-8} A/cm²) presented 1 order of magnitude higher, while Hybrid 20 (4.55×10^{-10} A/cm²) presented 1 order of magnitude lower compared to the pure Hybrid (6.32×10^{-9} A/cm²) with respect to corrosion current density.

According to Figure 4, the Hybrid 10 and Hybrid 40 samples have a higher concentration of titanium compared to silicon, which would justify the similar current density. The Hybrid 20 sample presents more of a barrier effect behavior, since the chemical mapping (Figure 4c) indicates greater silicon coverage compared to titanium. This indicates better barrier protection for this system, which consequently reduces the release of metal ions leached from the surface, which are associated with adverse reactions and cytotoxic effects on the human body⁵². Furthermore, it is worth noting that there is an optimal amount of silver concentration that favors the barrier effect of the hybrid film. This may be related to the better distribution of silver in the hybrid film. corrosion and helps maintain antibacterial activity for long periods of immersion in SBF, which means that in real situations silver reduces the probability of prosthesis rejection⁵³. On the other hand, excess silver can lead to saturation of the solution, since to reach approximately 80% of the amount of saturation in the solution, a certain time is required for the stability of the silver ions. However, after this saturation time, the silver ion release process may not be controlled, resulting in greater release and consequently reducing its electrochemical performance and causing contamination of the human body with silver residues.

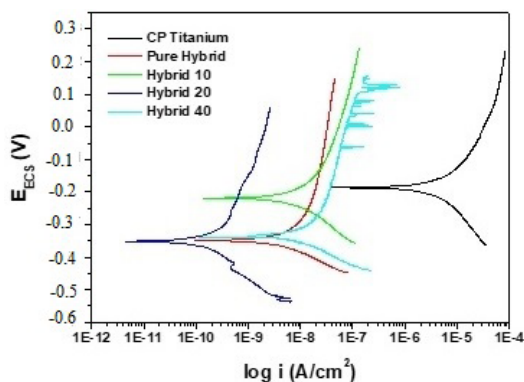


Figure 6. Potentiodynamic polarization curves of c.p. titanium and hybrid coatings.

Table 3. Simulation values for extrapolation of Tafel lines.

Sample	E_{corr} (mV)	i_{corr} (A/cm ²)	R_p (Ω/cm ²)
Titanium c.p.	-184	6.99×10^{-6}	5.85×10^2
Pure Hybrid	-348	6.32×10^{-9}	4.06×10^5
Hybrid 10	-218	1.19×10^{-8}	2.75×10^5
Hybrid 20	-349	4.55×10^{-10}	1.20×10^7
Hybrid 40	-338	1.18×10^{-8}	2.12×10^5

The concentrations used in this work were shown not to be excessive to the point of reducing corrosion resistance and causing contamination of the human body⁵⁴.

Authors found that the presence of silver increases corrosion resistance and helps maintain antibacterial activity for long periods of immersion in SBF, which means that in real situations silver reduces the probability of prosthesis rejection⁵⁵. On the other hand, excess silver can lead to saturation of the solution, since to reach approximately 80% of the amount of saturation in the solution, a certain time is required for the stability of the silver ions. However, after this saturation time, the silver ion release process may not be controlled, resulting in greater release and consequently reducing its electrochemical performance and causing contamination of the human body with silver residues. The concentrations used in this work were shown not to be excessive to the point of reducing corrosion resistance and causing contamination of the human body⁵⁶. The electrochemical information presented here should not be taken as absolute, for the following reasons: biomaterials, when inserted into the human body, may be susceptible to different voltages, making the situation more critical in terms of corrosion. Corrosion rate values may change due to conditions in the human body close to the implant, such as inflammatory processes. The biomaterial used in the implant may have a different chemical composition and manufacturing process than the material used in this work. The SBF solution only simulates a bodily fluid, but can be distinguished from the real solution.

3.5. Analysis of bactericidal and antifungal activity

Figure 7 shows the results of the bactericidal activity of the CP titanium, Pure Hybrid, Hybrid 10, Hybrid 20 and Hybrid 40 samples against *Escherichia coli*, *Staphylococcus aureus*, *Pseudomonas aeruginosa* and their antifungal activity against *Candida albicans*. These pathogens were selected due to their usual presence in surgical ward environments, and thus their coexistence with the titanium devices used in surgeries⁵⁵⁻⁶⁰.

Only in the case of *S. aureus* there was no inhibition of biofilm growth compared to the negative control. Regarding this bacterium, only the Hybrid 10 sample showed a slight inhibition when compared to the negative control. Furthermore, with respect to *E. coli*, the pure hybrid was not able to inhibit biofilm growth in relation to the negative control. The incorporation of silver nanoparticles seems to have favored the inhibition of biofilm growth in general. The great challenge in the development of coatings is to achieve an ideal performance balancing excellent biofunctionality and effective action against unwanted pathogens. In this context, as seen in Figure 7, it is evident that the Hybrid 10 sample showed the best performance, since it hampered the growth of the biofilm of all evaluated bacteria and fungi in relation to the negative control. In addition, the Hybrid 10 sample has greater roughness compared to CP titanium, consequently its coating allows a better compatibility for animal cells, which needs surface points to anchorage. However, microorganism are 30 -60 times lesser than animal cells. Then, the same roughness can be used by bacterial as local for hide and growth.

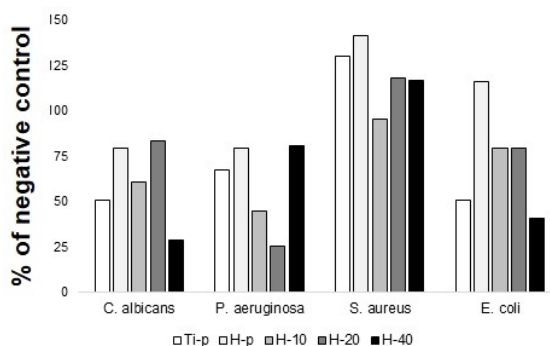


Figure 7. Evaluation of the biofilm growth of the coatings studied in relation to the percentage of the negative control.

There are two groups of bacteria, gram positive and gram negative. Among the bacteria tested in this study, *S. aureus* is gram-positive, while *E. coli* and *P. aeruginosa* are gram-negative. These two groups of bacteria are distinguished by the composition of their cell walls⁵⁷. The results of this study show that the bacteria most susceptible to the action of the silver nanoparticles in hybrid coatings are *E. coli* and *P. aeruginosa*, while *S. aureus* proved to be more resistant. In the literature, studies suggest that the effect of silver nanoparticles is more intense on gram-negative bacteria^{58,59}. This occurs because the silver nanoparticles act by attacking the peptidoglycan present in the cell wall. Therefore, it is more difficult to attack gram-positive bacteria, as they have a cell wall with a rigid and thick structure of about 30 nm, which makes it difficult for silver nanoparticles to penetrate into the interior of the cell. Silver nanoparticles attack gram-negative bacteria more easily, since the latter have a very thin layer, consisting of about 2 to 3 nm of peptidoglycan, and a layer of lipopolysaccharide studied silver nanoparticles with different sizes, 29 and 89 nm. They observed that there is a need for a greater amount of silver to inhibit the growth of *S. aureus* (gram-positive), compared to *E. coli* (gram-negative), due to the fact that silver nanoparticles have a more intense effect against gram-negative bacteria. Regarding the suppression of the *C. albicans* fungus, the sample with the best performance was Hybrid 40. However, it cannot be said that the silver nanoparticles inhibited biofilm growth for this species, as it is evident that the CP titanium surface without coating already hinders the development of the *C. albicans* biofilm. The initial adhesion of *C. albicans* depends on the surface topography⁵⁵. A smooth and homogeneous film makes it difficult for this fungus to adhere to the surface. On the other hand, a surface with deep cavities can stimulate the attachment of fungi and serve as an anchorage point for biofilm. That is, surface roughness may favor adhesion due to increased surface area⁵⁶. Since CP titanium had the surface with the least roughness, fungal adhesion may have been hampered.

4. Conclusion

Based on the results discussed, this study concludes that the synthetic route developed allowed the preparation of a polyurethane-siloxane-silver hybrid film with a reticulated

structure, and that the insertion of silver particles at the nanometric scale did not change the structural composition of the hybrid coatings. The SEM analyses of the pure samples and those with silver inserts revealed that the coating of the titanium using the Pure Hybrid generated a more regular surface with no microcracks in the film, covering the imperfections of the titanium surface. In the presence of small concentrations of silver ($6,92 \times 10^{-5}$ M of AgNPs (Hybrid 10), homogeneous a film was observed, without recesses and with slight discontinuities. However, when the concentration of silver nanoparticles was increased, a lack of interactions between the first and second layers of coating was observed. The results obtained by the roughness analysis using atomic force microscopy are consistent with the images obtained by SEM, with lower roughness indices for the pure sample in relation to the samples with the addition of silver nanoparticles. The data obtained from the potentiodynamic polarization process were also better when the titanium was covered with the coatings, since all of them provided a superior protective performance to the CP titanium. The Hybrid 20 sample presented lower corrosion current density and greater polarization resistance compared to the other samples, presenting a greater barrier effect due to the greater silicon coverage compared to titanium. The Hybrid 10 sample presented greater roughness compared to CP titanium, as well as a homogeneous film, resulting in a coating that allowed better compatibility and antibacterial activity. In relation to the results obtained, it can be concluded that, although Híbrido 10 presents better morphological and bacterial characteristics, the Híbrido 20 sample presented better electrochemical performance.

5. Acknowledgments

This work was carried out with the support of CNPq, a Brazilian government entity focused on human resources training. The authors also thank the financial support of Brazilian agencies: FAPERGS and FINEP. The authors would like to thank the Coordination for the Improvement of Higher Education Personnel - Brazil (CAPES / PROEX 88881.844968/2023/1061/2023) for the financial support.

6. References

- Rashti A, Yahyaei H, Firoozi S, Ramezani S, Rahiminejad A, Karimi R, et al. Development of novel biocompatible hybrid nanocomposites based on polyurethane-silica prepared by sol gel process. *Mater Sci Eng C*. 2016;69:1248-55.
- Braz AG, Pulcinelli SH, Santilli CV. Glycerol-based polyurethane-silica organic-inorganic hybrid as an anticorrosive coating. *Prog Org Coat*. 2022;169(1):106939.
- Zakaria FA, Hamidon TS, Hussin MH. Electrochemical and surface characterization studies of winged bean extracts doped TEOS-PDMS sol-gel protective coatings on reinforcing bar in acidic medium. *Ind Crops Prod*. 2023;202(1):117030.
- Xiong L, Liu J, Li Y, Li S, Yu M. Enhancing corrosion protection properties of sol-gel coating by pH-responsive amino-silane functionalized graphene oxide-mesoporous silica nanosheets. *Prog Org Coat*. 2019;135:228-39.
- Meera KMS, Sankar RM, Jaisankar SN, Mandal AB. Physicochemical studies on polyurethane/siloxane cross-linked films for hydrophobic surfaces by the sol-gel process. *J Phys Chem B*. 2013;117(9):26822694.
- Lutzler T, Charpentier TVJ, Barker R, Soltanahmadi S, Taleb W, Wang C, et al. Evaluation and characterization of anti-corrosion properties of sol-gel coating in CO₂ environments. *Mater Chem Phys*. 2018;216(1):272-7.
- Ji X, Wang W, Zhao X, Wang L, Ma F, Wang Y, et al. Poly (dimethyl siloxane) anti-corrosion coating with wide pH-responsive and self-healing performance based on core-shell nanofiber containers. *J Mater Sci Technol*. 2022;101:128-45.
- Harb SV, Cerrutti BM, Pulcinelli SH, Santilli CV, Hammer P. Siloxane-PMMA hybrid anti-corrosion coatings reinforced by lignin. *Surf Coat Tech*. 2015;275:9-16.
- Yu Q, Wu Z, Chen H. Dual-function antibacterial surfaces for biomedical applications. *Acta Biomed*. 2015;16:113.
- Kaur R, Liu S. Antibacterial surface design - contact Kill. *Prog Surf Sci*. 2016;91(3):136-53.
- Querido MM, Aguiar L, Neves P, Pereira CC, Teixeira JP. Self-disinfecting surfaces and infection control. *Colloids Surf B Biointerfaces*. 2019;178:8-21.
- Hajipour MJ, Fromm KM, Ashkarran AA, Aberasturi DJ, Larramendi IR, Rojo T, et al. Antibacterial properties of nanoparticles. *Trends Biotechnol*. 2012;30(10):499-511.
- Tripathy A, Sen P, Su B, Briscoe WH. Natural and bioinspired nanostructured bactericidal surfaces. *Adv Colloid Interface Sci*. 2017;248:85-104.
- Hasan J, Crawford RJ, Ivanova EP. Antibacterial surfaces: the quest for a new generation of biomaterials. *Trends Biotechnol*. 2013;31(5):295-304.
- Nguyenova HY, Yokata B, Zaruba K, Siegel J, Kolska Z, Svorcik V, et al. Silver nanoparticles grafted onto PET: effect of preparation method on antibacterial activity. *React Funct Polym*. 2019;145:104376.
- Hekmati M, Hasanirad S, Khaledi A, Esmaili D. Green synthesis of silver nanoparticles using extracts of *Allium rotundum* L, *Falcaria vulgaris* Bernh, and *Ferulago angulate* Boiss, and their antimicrobial effects in vitro. *Gene Rep*. 2020;19:100589.
- Kotanan S, Laaksonen T, Sarlin E. Feasibility of polyamines and cyclic carbonate terminated prepolymers in polyurethane/polyhydroxyurethane synthesis. *Mater Today Commun*. 2020;23:100863.
- Mohammadi A, Doctorsafaei AH, Burujeny SB, Rudbari HA, Kordestani N, Najafabadi SAA. Silver (I) complex with a Schiff base ligand extended waterborne polyurethane: a developed strategy to obtain a highly stable antibacterial dispersion impregnated with in situ formed silver nanoparticles. *Chem Eng J*. 2020;381:122776.
- Melo MA Jr, Santos LSS, Gonçalves MC, Nogueira AF. Preparação de nanopartículas de prata e ouro: um método simples para a introdução da nanociência em laboratório de ensino. *Quim Nova*. 2012;35(9):1872-8.
- Certhoux E, Ansart F, Turq V, Bonino JP, Sobrino JM, Garcia J, et al. New sol-gel formulations to increase the barrier effect of a protective coating against the corrosion of steels. *Prog Org Coat*. 2013;76(1):165-72.
- Akram D, Hakami O, Sharmin E, Ahmad S. Castor and Linseed oil polyurethane/TEOS hybrids as protective coatings: a synergistic approach utilising plant oil polyols, a sustainable resource. *Prog Org Coat*. 2017;108:1-14.
- Eaton P, Holmes P, Yarwood J. In situ ATR-FTIR and Raman microscopic studies of organosilane hydrolysis and the effect of hydrolysis on silane diffusion through a polymeric film. *J Appl Polym Sci*. 2001;82(8):2016-26.
- Mohammadi I, Shahrabi T, Mahdavian M, Izadi M. A novel corrosion inhibitive system comprising Zn-Al LDH and hybrid sol-gel silane nanocomposite coating for AA2024-T3. *J Alloys Compd*. 2022;909:164755.

24. Salvador DG, Marcolin P, Beltrami LVR, Brandalise RN, Kunst SR. Influence of the pretreatment and curing of alkoxy silanes on the protection of the titanium-aluminum-vanadium alloy. *J Appl Polym Sci.* 2017;134(46):45470.
25. Li J, Wang L, Bai H, Chen C, Liu L, Guo H, et al. Development of an eco-friendly waterborne polyurethane/catecholamine/sol-gel composite coating for achieving long-lasting corrosion protection on Mg alloy AZ31. *Prog Org Coat.* 2023;183:107732.
26. Franquet A, Terryn H, Vereecken J. IRSE study on effect of thermal curing on the chemistry and thickness of organosilane films coated on aluminium. *Appl Surf Sci.* 2003;11:259-69.
27. De Graeve I, Vereecken J, Franquet A, van Schaffinghen T, Terryn H. Silane coating of metal substrates: complementary use of electrochemical, optical and thermal analysis for the evaluation of film properties. *Prog Org Coat.* 2007;59(3):224-9.
28. Romano AP, Fedel M, Deflorian FD, Olivier MG. Silane sol-gel film as pretreatment for improvement of barrier properties and filiform corrosion resistance of 6016 aluminum alloy covered by cathodic coating. *Prog Org Coat.* 2011;72(4):695-702.
29. Abdulsada FW, Hammood AS. Characterization of corrosion and antibacterial resistance of hydroxyapatite/silver nanoparticles powder on 2507 duplex stainless steel. *Mater Today.* 2021;42:23012307.
30. Palza H. Antimicrobial polymers with metal nanoparticles. *Int J Mol Sci.* 2015;16(1):2099-116.
31. Chen J, Wang J, Yuan H. Morphology and performances of the anodic oxide films on Ti_6Al_4V alloy formed in alkaline-silicate electrolyte with aminopropyl silane addition under low potential. *Appl Surf Sci.* 2013;284:900-6.
32. Catauro M, Bollino F, Papale F, Giovanardi R, Veronesi P. Corrosion behavior and mechanical properties of bioactive sol-gel coatings on titanium implants. *Mater Sci Eng C.* 2014;43:375-82.
33. Diener A, Nebe B, Lüthen F, Becker P, Beck U, Neumann HG, et al. Control of focal adhesion dynamics by material surface characteristics. *Biomaterials.* 2005;26(4):383-92.
34. Rodríguez-Cano A, Cintas P, Fernández-Calderón M, Pacha-Olivencia M, Crespo L, Saldaña L, et al. Controlled silanization-amination reactions on the $Ti6Al4V$ surface for biomedical applications. *Colloids Surf B Biointerfaces.* 2013;106:248-57.
35. Deflorian F, Rossi S, Fedrizzi L. Silane pre-treatments on copper and aluminium. *Electrochim Acta.* 2006;51(27):6097-103.
36. Ramezanzadeh B, Raeisi E, Mahdavian M. Studying various mixtures of 3-aminopropyltriethoxysilane (APS) and tetraethylorthosilicate (TEOS) silanes on the corrosion resistance of mild steel and adhesion properties of epoxy coating. *Int J Adhes Adhes.* 2015;63(9):166-76.
37. He G, Li Y, Li Z, Nie L, Wu H, Yang X, et al. Enhancing water retention and low-humidity proton conductivity of sulfonated poly(ether ether ketone) composite membrane enabled by the polymer-microcapsules with controllable hydrophilicity-hydrophobicity. *J Power Sources.* 2014;248:951-61.
38. Kayani ZN, Anwar M, Saddiqe Z, Riaz S, Naseem S. Biological and optical properties of sol-gel derived ZnO using different percentages of silver contents. *Colloids Surf B Biointerfaces.* 2018;171:383-90.
39. Wypych G. *Handbook of plasticizers.* 2nd ed. Ontario: Chemtec Publishing; 2012. 800 p.
40. Di H, Qiaoxia L, Yujie Z, Jingxuan L, Yan W, Yinchun H, et al. Ag nanoparticles incorporated tannic acid/nanoparticle composite coating on Ti implant surfaces for enhancement of antibacterial and antioxidant properties. *Surf Coat Tech.* 2020;399:126169.
41. Marino CEB, Rocha-Filho RC, Bocchi N, Biaggio SR. Investigaç o da estabilidade de materiais biocompat veis por an lise microestrutural. In: 23^a Reuni o Anual da Sociedade Brasileira de Qu mica. Anais. Poços de Caldas: PubliSBQ; 2000. n. 0301.
42. Brooks EK, Brooks RP, Ehrensberger MT. Effects of simulated inflammation on the corrosion of 316L stainless steel. *Mater Sci Eng C.* 2017;71:200-5.
43. Zhang XF, Liu ZG, Shen W, Gurunathan S. Silver nanoparticles: synthesis, characterization, properties, applications, and therapeutic approaches. *Int J Mol Sci.* 2016;17(9):1534.
44. Seyfi J, Goodarzi V, Wurm FR, Shojaei S, Jafari-Nodoushan M, Najmuddin N, et al. Developing antibacterial superhydrophobic coatings based on polydimethylsiloxane/silver phosphate nanocomposites: assessment of surface morphology, roughness and chemistry. *Prog Org Coat.* 2020;149:105944.
45. Longhi MC, Casagrande Rb, Kunst SR, Santos VD, Ferreira JZ. Obtainment and characterization of a silicon alkoxides-based coating applied to a substrate of stainless steel 316L for use in biomaterials. *Mater Res.* 2019;22(3):e20180514.
46. Anderson JA, Lamichhane S, Mani G. Macrophage responses to 316L stainless steel and cobalt chromium alloys with different surface topographies. *J Biom Mat Resear - Part A.* 2016;104(11):26582672.
47. Yan Y, Chibowski E, Szcze s A. Surface properties of ti-6al-4v alloy part i: surface roughness and apparent surface free energy. *Mater Sci Eng C.* 2017;70:207-15.
48. Ramires I, Guastaldi AC. Estudo do biomaterial Ti-6Al-4V empregando-se t cnicas eletroqu micas e XPS. *Quim Nova.* 2002;25(1):10-4.
49. Dalmau A, Guin n Pina V, Devesa F, Amig  V, Igual Mu oz A. Influence of fabrication process on electrochemical and surface properties of Ti-6Al-4V alloy for medical applications. *Electrochim Acta.* 2013;95:102-11.
50. Masters EA, Ricciardi BF, Bentley KLM, Moriarty TF, Schwarz EM, Muthukrishnan G. Skeletal infections: microbial pathogenesis, immunity and clinical management. *Nat Rev Microbiol.* 2022;20(7):385-400.
51. R go GC, Bandeira RM, van Drunen J, Tremiliosi-Filho G, Casteletti LC. Multi-layer organic-inorganic hybrid anticorrosive coatings for protection of medium carbon steel. *Mater Chem Phys.* 2023;303(2):127841.
52. Mazare A, Anghel AC, Surdu-Bob G, Totea ID, Demetrescu I, Ionita D. Silver doped diamond-like carbon antibacterial and corrosion resistance coatings on titanium. *Thin Solid Films.* 2018;657:16-23.
53. Akhavan O. Lasting antibacterial activities of Ag-TiO₂/Ag/a-TiO₂ nanocomposite thin film photocatalysts under solar light irradiation. *J Colloid Interface Sci.* 2009;336(1):117-24.
54. Cremasco A, Andrade PN, Contieri RJ, Lopes ESN, Afonso CRM, Caram R. Correlations between aging heat treatment, ω phase precipitation and mechanical properties of a cast Ti-Nb alloy. *Mater Des.* 2011;32(4):2387-90.
55. Wang J, An Y, Liang H, Tong Y, Guo T, Ma C. The effect of different titanium nitride coatings on the adhesion of *Candida albicans* to titanium. *Arch Oral Biol.* 2013;58(10):1293-301.
56. Cerioli M, Batailler C, Conrad A, Roux S, Perpoint T, Becker A, et al. *Pseudomonas aeruginosa* Implant-associated bone and joint infections: experience in a regional reference center in France. *Front Med.* 2020;7(7):513242.
57. Cobo F, Rodr guez-Granger J, L pez EM, Jim nez G, Sampedro A, Aliaga-Mart nez L, et al. *Candida*-induced prosthetic joint infection: a literature review including 72 cases and a case report. *Infect Dis.* 2017;49(2):81-94.
58. Saconi ES, Carvalho VC, Oliveira PRD, Lima ALLM. Prosthetic joint infection due to *Candida* species: case series and review of literature. *Medicine.* 2020;99(15):e19735.
59. Metsemakers WJ, Kuehl R, Moriarty TF, Richards RG, Verhofstad MHJ, Borens O, et al. Infection after fracture fixation: current surgical and microbiological concepts. *Injury.* 2018;49(3):511-22.
60. Pri  H, Meyssonier V, Kerroumi Y, Heym B, Lidove O, Marmor S, et al. *Pseudomonas aeruginosa* prosthetic joint-infection outcomes: Prospective, observational study on 43 patients. *Front Med.* 2022;9(9):1039596.